Heat activation is intrinsic to the pore domain of TRPV1

Feng Zhang[a], Andres Jara-Oseguera[a], Tsg-Hui Chang[a], Chanhyung Bae[a], Sonya M. Hanson[a,1], and Kenton J. Swartz[a,2]

[a]Molecular Physiology and Biophysics Section, Porter Neuroscience Research Center, National Institute of Neurological Disorders and Stroke, National Institutes of Health, Bethesda, MD 20892

Edited by Ardem Patapoutian, Scripps Research Institute, La Jolla, CA, and approved November 30, 2017 (received for review September 29, 2017)

The TRPV1 channel is a sensitive detector of pain-producing stimuli, including noxious heat, acid, inflammatory mediators, and vanilloid compounds. Although binding sites for some activators have been identified, the location of the temperature sensor remains elusive. Using available structures of TRPV1 and voltage-activated potassium channels, we engineered chimeras wherein transmembrane regions of TRPV1 were transplanted into the Shaker Kv channel. Here we show that transplanting the pore domain of TRPV1 into Shaker gives rise to functional channels that can be activated by a TRPV1-selective tarantula toxin that binds to the outer pore of the channel. This pore-domain chimera is permeable to Na^+, K^+, and Ca^{2+} ions, and remarkably, is also robustly activated by noxious heat. Our results demonstrate that the pore of TRPV1 is a transportable domain that contains the structural elements sufficient for activation by noxious heat.

capsaicin | transient receptor potential | thermosensing | tarantula toxin | DkTx

Temperature-sensitive transient receptor potential (TRP) channels play critical biological roles in sensing heat and cold (1, 2). The vanilloid-sensitive TRPV1 channel can be activated by noxious or pain-producing stimuli, including heat, vanilloids such as capsaicin from hot chili peppers, extracellular acid, and venom toxins (3). Vanilloids bind to the intracellular ends of the S3–S6 transmembrane (TM) helices, whereas the TRPV1-specific double-knot toxin (DkTx) from tarantula venom and protons bind to the extracellular end of the pore formed by the S5–S6 helices (4–6). In contrast, localizing the temperature-sensing elements within TRPV1, as well as those within all other temperature-activated TRP channels, has not yet been achieved (1). Recordings of purified TRPV1 channels reconstituted into artificial liposomes suggest that the protein is intrinsically heat sensitive (7), and manipulating the lipid and cholesterol composition of native membranes suggests that lipids likely do not play a critical role in temperature sensing (8). In contrast, mutagenesis or deletion studies have identified several regions that are important for heat-dependent activation throughout TRPV1 and other heat-activated TRP channels. These regions include the N-terminal ankyrin repeat domains in TRPA1 (9), a membrane-proximal N-terminal segment for TRPV1, TRPV2, and TRPV3 (10, 11), the C terminus of TRPV1 (12–15), and the pore domain in TRPV1 (16–19), TRPV3 (20), and TRPA1 (21, 22) channels. Indeed, it has been proposed that residues involved in temperature sensing may be scattered throughout the receptor rather than forming a defined temperature-sensing domain (23). Although these studies identify regions of the protein where manipulations alter heat activation, it remains unclear whether they contribute directly to temperature sensing or have other roles in allosteric coupling or opening and closing of the pore. Furthermore, truncation of most of the N and C termini of TRPV1 cannot be achieved without losing channel function (13, 24), so it has not been possible to evaluate whether the cytoplasmic domains are essential for the temperature-sensing mechanism. We were particularly interested in exploring the role of the pore domain of TRPV1 in temperature sensing because heat activation of the channel is exquisitely sensitive to binding of Na^+, H^+, or DkTx to the external pore (19, 25). In the present study, we take advantage of the overall structural similarities of the pore domains of TRPV1 and voltage-activated K^+ channels (4, 26) to generate chimeras in which the pore domain of TRPV1 was transferred into the Shaker K^+ channel. We succeeded in generating functional chimeras, one of which can be activated by TRPV1-selective tarantula toxins, displays Ca^{2+} permeability and remarkably can also be activated by noxious heat with similar sensitivity to that of the TRPV1 channel.

Results

If the pore domain of TRPV1 contains the temperature sensor, we reasoned that it may be possible to generate heat-activated chimeras by transplanting the pore domain of TRPV1 into a structurally related channel whose activity lacks strong temperature sensitivity. To test this idea, we selected the Shaker K^+ channel, a well-studied voltage-activated K^+ (Kv) channel that is relatively temperature insensitive (27), making it an excellent background in which to evaluate temperature-sensitive elements in TRPV1. Alignment of the crystal structure of a channel construct closely related to Shaker, the Kv1.2/2.1 paddle chimera (26), to a cryo-EM structure of TRPV1 (4) reveals that the backbone of their integral membrane domains (S1–S6) is remarkably similar, with especially low C_α rmsd (2.5 Å) and high TM score (0.75) within the pore-forming regions (Fig. 1*A* and *Materials and Methods*) (28). Using backbone superposition of the TRPV1 and Kv1.2/2.1 structures to align the primary sequences of TRPV1 and the Shaker Kv channel (Fig. 1*A* and *Materials and Methods*), we designed chimeras in which varying portions of the S1–S6 helices were transplanted between Shaker and TRPV1 (Fig. S1). We then expressed each of the chimeras in *Xenopus* oocytes and tested for activation of membrane currents in response to voltage steps or to the extracellular application of a more potent variant of DkTx that contains two high-affinity K2 knot (K2K2) (5). Although most chimeras failed to give rise to functional channels, we identified one functional chimera in

Significance

The TRPV1 channel is an important detector of noxious heat, yet the location of the heat sensor and the mechanism of heat activation remain poorly understood. Here we used structure-based engineering between the heat-activated TRPV1 channel and the Shaker Kv channel to demonstrate that transplantation of the pore domain of TRPV1 into Shaker gives rise to functional channels that can be activated by a TRPV1-selective tarantula toxin and by noxious heat, demonstrating that the pore of TRPV1 contains the structural elements sufficient for activation by temperature.

Author contributions: F.Z., A.J.-O., S.M.H., and K.J.S. designed research; F.Z., A.J.-O., T.-H.C., and C.B. performed research; C.B. contributed new reagents/analytic tools; F.Z., A.J.-O., T.-H.C., and C.B. analyzed data; and F.Z., A.J.-O., T.-H.C., and K.J.S. wrote the paper.

The authors declare no conflict of interest.

This article is a PNAS Direct Submission.

[1]Present address: Computational Biology Program, Memorial Sloan Kettering Cancer Center, New York, NY 10065.

[2]To whom correspondence should be addressed. Email: Kenton.Swartz@nih.gov.

This article contains supporting information online at www.pnas.org/lookup/suppl/doi:10.1073/pnas.1717192115/-/DCSupplemental.

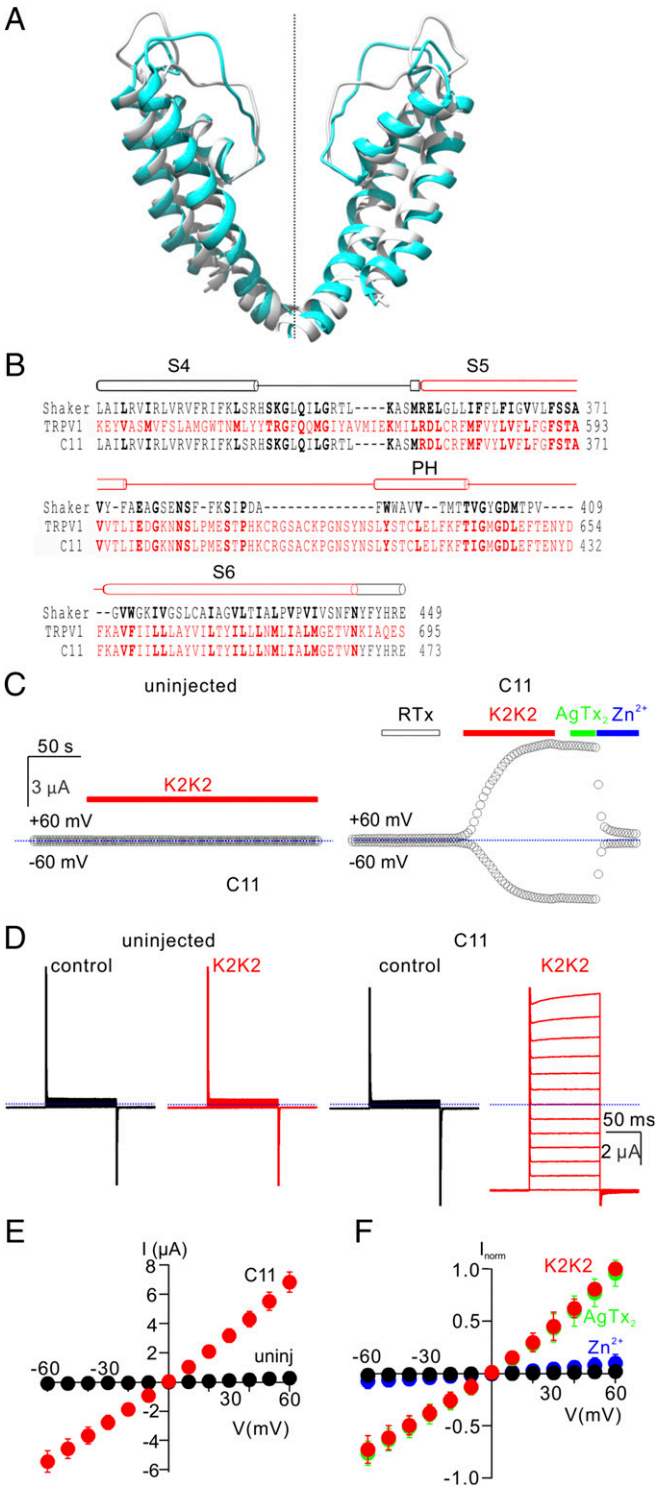

Fig. 1. Transfer of the pore domain from TRPV1 into the Shaker Kv channel. (*A*) Backbone superposition of the pore domains of the Kv1.2/2.1 paddle chimera (gray; PDB ID code 2R9R) and RTx/DkTx-bound TRPV1 (cyan; PDB ID code 5IRX) using TM align (28). Backbone rmsd = 2.5 Å and TM score = 0.75. (*B*) Structure-based sequence alignment of Shaker (black), TRPV1 (red), and the C11 pore chimera in the transmembrane region spanning from S4 through S6 with conserved residues shown in bold. (*C*) Representative time courses for recording membrane currents at −60 and +60 mV from an uninjected oocyte (*Left*; control) and an oocyte injected with the C11 chimera (*Right*). Cells were held at −60 mV and voltage was stepped to +60 mV for 100 ms at 3-s intervals. Mean inward current at −60 mV (*Lower* symbols) and outward current at +60 mV (*Upper* symbols) are plotted vs. time. RTx (100 nM), K2K2 (5 μM), AgTx-2 (100 nM), and Zn^{2+} (2 mM) were applied to the extracellular solution as indicated by horizontal bars. Dotted blue lines denote the zero-current level. The external recording solution contained (in millimoles/liter): 100 KCl, 10 Hepes, 2 $MgCl_2$, pH7.4. (*D*) Representative current traces from control (*Top*) and C11 chimera (*Bottom*) before (*Left*) and after (*Right*) the addition of 5 μM K2K2 (V_{hold} = −60 mV; test depolarizations from −60 to +60 mV in 10-mV increments). (*E*) I–V relations for membrane currents recording in the presence of 5 μM K2K2 in control uninjected oocytes (black symbols) and C11 injected oocytes (red symbols) obtained from experiments as in *D* (mean ± SEM for $n = 4$). (*F*) Normalized I–V relations before (black symbols) and after K2K2 application (5 μM, red symbols), followed by application of AgTx-2 (100 nM, green symbols) and then Zn^{2+}(2 mM, blue symbols), obtained from experiments as in *D*. Currents were normalized to the amplitude of current in the presence of 5 μM K2K2 at +60 mV (mean ± SEM for $n = 7$).

which the entire S5–S6 region was transferred from TRPV1 into Shaker (C11) (Fig. 1*B*) and another including an additional short extension past the C terminus of the TRPV1 S6 helix (C9) (Fig. S1). We chose to focus on the smaller C11 chimera, which exhibited robust activation of membrane currents in response to K2K2 application, with relatively linear current–voltage (I–V) relations (Fig. 1 *C*–*E*). Both Shaker and the C11 chimera traffic to the plasma membrane, as surface biotinylation of intact cells with a membrane-impermeant reagent led to specific streptavidin-mediated pulldown of the proteins following detergent solubilization (Fig. S2). The C11 chimera could also be activated by DkTx (Fig. S3 *A* and *B*), but not by the vanilloid resiniferatoxin (RTx) (Fig. 1*C*), as expected because this chimera does not contain the most critical residues for vanilloid sensitivity (29). The C11 chimera was inhibited by ruthenium red (RR), a nonspecific inhibitor of TRPV1 channels (30), although the extent of inhibition was less for C11 compared with TRPV1 (Fig. S3*C*). In addition, extracellular Zn^{2+} inhibited TRPV1 and the C11 chimera with similar affinity but had no apparent effect on Shaker (Fig. 1 *C* and *F* and Fig. S4 *A*–*D*), suggesting that the metal binds within the pore domain of TRPV1. The C11 chimera was not blocked by Agitoxin-2 (AgTx-2; Fig. 1 *C* and *F*), a selective pore-blocker of Shaker (31, 32), confirming that the functional pore of the chimera is derived from TRPV1 rather than Shaker. We also expressed the C11 chimera in HEK cells, and observed that cells looked unhealthy within 24 h and that it was not possible to obtain the GΩ seals required for stable whole-cell recordings. Because oocytes better tolerate the expression of Ca^{2+} permeable channels on their plasma membrane, and expression levels can be readily controlled by titrating the concentration of cRNA injected, we used oocytes for further characterization of the C11 chimera.

Although our results thus far demonstrate that the C11 chimera forms functional ion channels, we were concerned that the structure of the permeation pathway might be distorted compared with TRPV1. The TRPV1 channel is considerably more permeable to small monovalent cations such as Na^+ or K^+ compared with the larger organic cation *N*-methyl-D-glucamine ($NMDG^+$) and is even more permeable to Ca^{2+} (30, 33). To investigate the ion selectivity of the C11 chimera, we first obtained I–V relations in the presence of either external K^+, Na^+, or $NMDG^+$ (all in the absence of Ca^{2+}) after activating the channel with K2K2. For both TRPV1 and the C11 chimera, I–V relations reversed at V_{rev} values close to 0 mV in external solutions containing 100 mM K^+ or Na^+ (Fig. 2 *A* and *B* and Fig. S4 *E* and *F*), as expected because the internal K^+ concentration in these cells is about 100 mM and the TRPV1 channel has similar permeability to Na^+ or K^+ ions (30). We then replaced external K^+ with $NMDG^+$ and observed large shifts of the I–V relations to negative voltages for TRPV1 and the C11 chimera (Fig. 2 *A* and *B*), indicating that both channels are considerably more permeable to K^+ compared with $NMDG^+$. To test whether the C11 chimera was permeable to Ca^{2+}, we examined whether its activation would allow Ca^{2+} to enter oocytes and open Ca^{2+}-activated

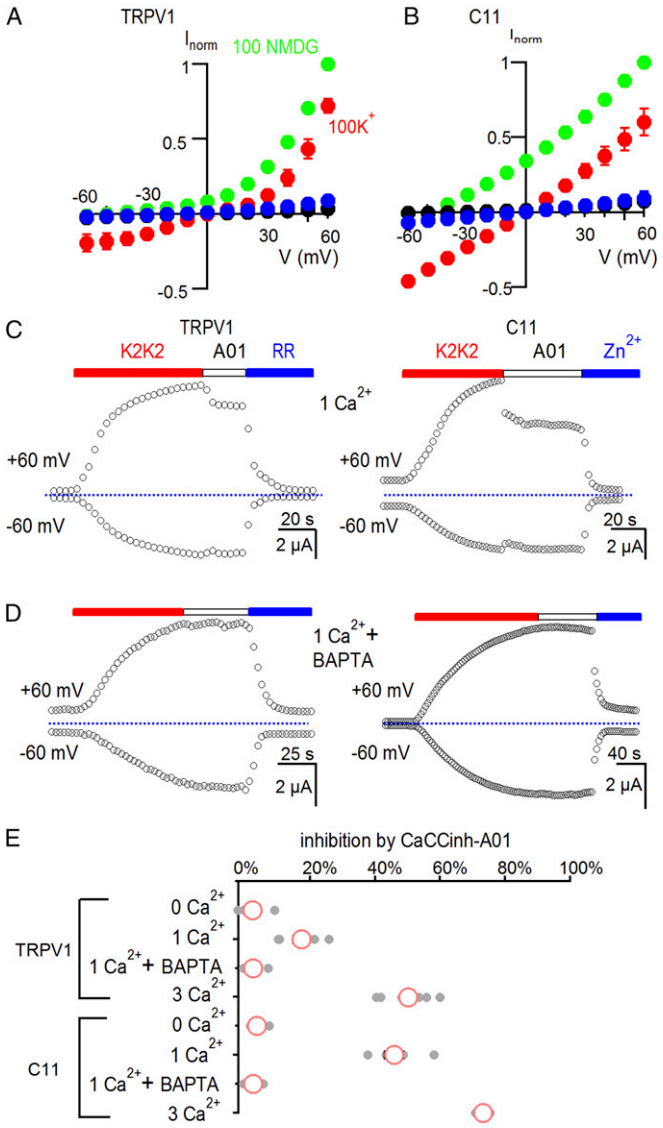

Fig. 2. The C11 chimera is calcium permeable. (*A*) I–V relations for TRPV1-expressing cells before (black) and after application of 5 μM K2K2 in 100 mM K^+ (red), 100 mM $NMDG^+$ (green), or after application of 50 μM RR in 100 mM K^+ (blue). Symbols are mean ± SEM for $n = 5$. (*B*) I–V relations for C11-expressing cells before (black) and after application of 5 μM K2K2 in 100 mM K^+ (red), 100 mM $NMDG^+$ (green), or after application of 2 mM Zn^{2+} in 100 mM K^+ (blue). Symbols are mean ± SEM for $n = 5$. (*C*) Time course for activation of membrane currents following extracellular application of K2K2 and testing for inhibition by the calcium-activated chloride channel inhibitor CaCCinh-A01(A01) for cells expressing TRPV1 (*Left*) or the C11 chimera (*Right*). The external solution had 1 mM Ca^{2+}. Cells were held at −60 mV, and voltage was stepped to +60 mV for 100 ms every 3 s. TRPV1 was subsequently inhibited by RR (50 μM; *Left*) and the C11 chimera by Zn^{2+} (2 mM; *Right*). The dotted horizontal line indicates the zero-current level. (*D*) Injecting cells with BAPTA eliminates the A01-dependent reduction in membrane current in the presence of 1 mM external Ca^{2+}. (*E*) Summary of inhibition of K2K2-activated membrane current at +60 mV by 30 μM CaCCinh-A01 under different conditions. Data points for individual cells are shown as gray circles, and the mean ± SEM ($n = 4$–7) as red circles and black bars, respectively. The concentration of external Ca^{2+} is indicated in millimoles/liter.

Cl^- channels that are native to these cells (34). When cells expressing TRPV1 or the C11 chimera were placed in solutions containing external Ca^{2+} ions, the Ca^{2+}-activated Cl^- channel inhibitor Caccinh-A01 (abbreviated A01) (35) inhibited a fraction of the K2K2-activated membrane current (Fig. 2 *C* and *E*). In contrast, A01 had no detectable effect when the external solution did not contain Ca^{2+} ions, or when cells were injected with the Ca^{2+} chelator BAPTA (Fig. 2 *D* and *E*). From these results, we conclude that the C11 chimera is Ca^{2+} permeable.

The C11 chimera retains the S1–S4 voltage-sensing domains from Shaker, yet macroscopic currents measured for C11 exhibited little voltage dependence (Fig. 1 *D* and *E*), suggesting that the voltage sensors are not tightly coupled to the pore domain in this chimera. Tight packing between the internal end of S6 and the S4–S5 linker has been shown to be critical for such coupling in Kv channels (36, 37), and these contacts would likely be disrupted in the C11 chimera because it contains the S6 helix from TRPV1 and an S4–S5 linker helix from Shaker. To explore whether the S1–S4 domain has any functional role in the C11 chimera, we investigated the impact of modifying the S3b–S4 voltage-sensor paddle motif (38–41). Neutralization of the outer three S4 Arg residues in Shaker leads to constitutive activation of the channel (42, 43), suggesting that these S4 charges are required for negative membrane voltages to drive the voltage sensors into resting states and to close the pore. The S3b–S4 paddle motif in Shaker contains the three outer S4 Arg residues, and when we replaced the paddle of Shaker with the corresponding region of TRPV1 to generate chimera 21, we observed constitutive activation of the channel that could be fully inhibited by AgTx-2 (Fig. 3 *A*–*C*). We then made the same replacement of the S3b–S4 paddle of Shaker in the background of C11 to generate the C23 chimera and observed K2K2-activated currents that were indistinguishable from those of the C11 chimera (Fig. 3 *A* and *D*–*F*). This result is important because it suggests that S1–S4 voltage-sensing domains of Shaker do not have detectable influence on the pore domain of TRPV1, as if Shaker simply serves as a scaffold for expressing functional pore domains of TRPV1 to the plasma membrane. We note that both the C11 and C23 chimeras exhibited small voltage-dependent relaxations at the most positive membrane voltages studied (see Fig. 1*D* for C11 and Fig. 3*E* for C23), suggesting that the weak voltage sensitivity that is a hallmark of TRPV1 (44) may be partly maintained in the C11 chimera.

The results thus far show that transfer of the pore domain of TRPV1 into Shaker gives rise to small-cation selective channels that can be activated by K2K2. To explore whether the pore domain of TRPV1 contains the necessary elements for sensing noxious heat, we undertook temperature-activation experiments on control cells not expressing exogenous channels and compared them with those expressing either TRPV1 or the C11 chimera. We observed robust activation of membrane currents by heat for cells expressing TRPV1 (Fig. 4 *A*–*C*), consistent with earlier studies (30). In contrast, we observed little if any activation of membrane currents in uninjected cells (Fig. 4 *D*–*F*), or cells expressing either Shaker (Fig. S5 *A*–*C*) or Shaker ILT (Fig. S5 *D* and *E*), a Shaker mutant reported to facilitate observation of intrinsic temperature-dependent gating (45). Remarkably, expression of the C11 chimera gave rise to robust activation of membrane currents by noxious heat (Fig. 4 *G*–*I*), and these could be reversed by subsequent cooling or inhibited by extracellular application of Zn^{2+} while maintaining the heat stimulus (Fig. 4 *J* and *K*). In addition, the C23 chimera lacking the three outer S4 Arg residues retained robust activation by noxious heat (Fig. 4 *L*–*N*), confirming that the voltage-sensing domains in Shaker do not play an important role in the sensitivity of these chimeras to heat. To compare the steepness of temperature-activation relations for TRPV1 and the chimeras in a semiquantitative manner, we determined Q_{10} values for activation of membrane currents above 36 °C and obtained values of 26 ± 7.4 for TRPV1, 40.8 ± 7.5 for the C11 chimera, and 29.8 ± 9.7 for the C23 chimera (Fig. 4 *C*, *I*, and *N*), values that are in agreement with reported heat

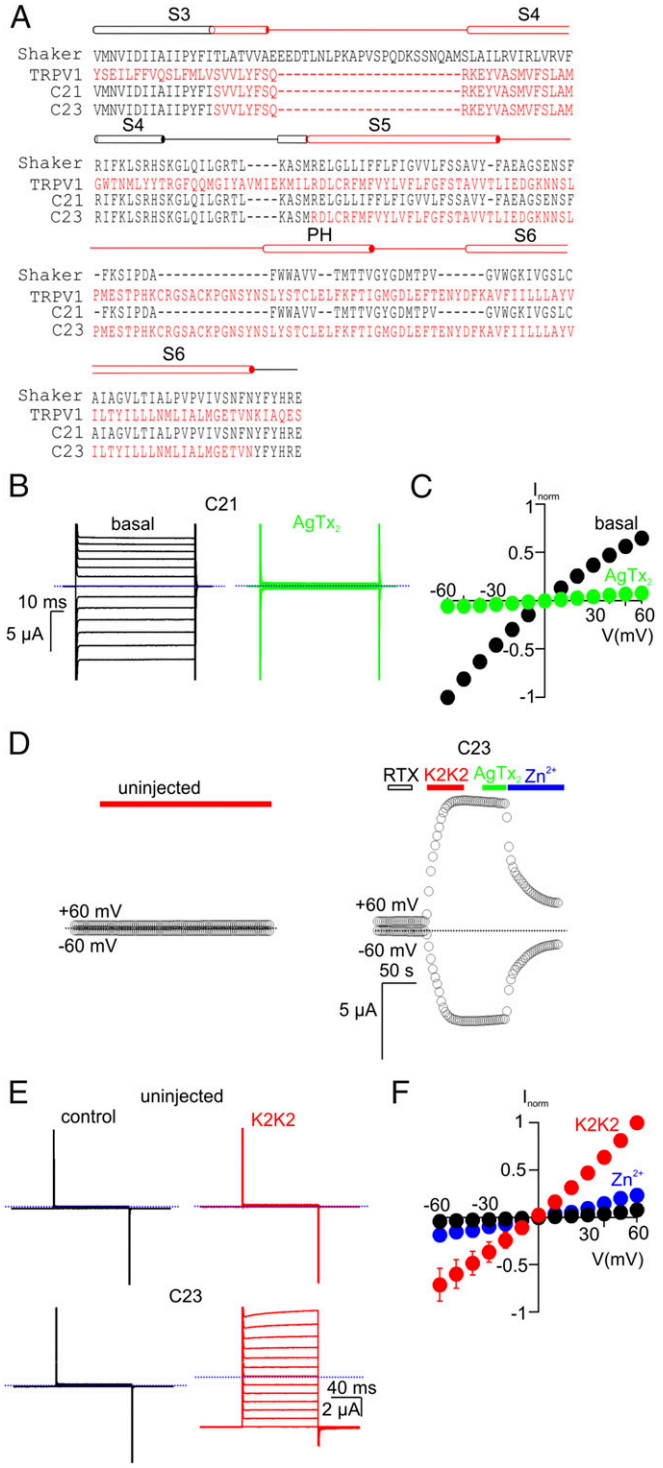

Fig. 3. Transfer of the paddle motif from TRPV1 into the C11 chimera does not alter its functional properties. (*A*) Sequence alignment of Shaker (black), TRPV1 (red), and the C21 and C23 chimeras from S3 through S6. (*B*) Representative current traces from cells expressing C21 before (*Left*) and after (*Right*) the addition of 100 nM AgTx-2 (V_{hold} = 0 mV; test depolarizations from −60 to +60 mV in 10-mV increments). (*C*) Normalized I–V relations obtained in the absence (black symbols) or presence of AgTx-2 (100 nM, green symbols) obtained from experiments as in *B*. Currents were normalized to the amplitude of current at −60 mV in control solutions (mean ± SEM for n = 5). (*D*) Representative time courses for membrane currents recorded at −60 and +60 mV from an uninjected oocyte (*Left*; control) and an oocyte injected with the C23 chimera (*Right*). Cells were held at V_{hold} = −60 mV and voltage was stepped to +60 mV for 100 ms at 3-s intervals. Mean inward current at −60 mV and outward current at +60 mV are plotted as a function of time. RTx (100 nM), K2K2 (5 μM), AgTx-2 (100 nM), and Zn^{2+} (2 mM) were applied as indicated by the horizontal bars. The dotted blue lines denote the zero-current level. The external recording solution contained (in millimoles/liter): 100 KCl, 10 Hepes, 2 $MgCl_2$, pH 7.4. (*E*) Representative current traces from an uninjected cell (*Top*) and a C23-expressing cell (*Bottom*) before (*Left*) and after (*Right*) the addition of 5 μM K2K2 (V_{hold} = −60 mV; test depolarizations from −60 to +60 mV in 10-mV increments). (*F*) Normalized I–V relations before (black symbols) and after K2K2 application (5 μM, red symbols), followed by Zn^{2+} application (2 mM, blue symbols), obtained from experiments as in *E*. Currents were normalized to the amplitude of current in the presence of 5 μM K2K2 at +60 mV (mean ± SEM for n = 4).

sensitivities of TRPV1 in this temperature range (8, 19, 46). In contrast, the steepness of the relations for cells expressing TRPV1, C11, or C23 at lower temperatures (~15–30 °C; where leak currents make a major contribution to the recorded currents), was very small and similar to the Q_{10} values at T > 37 °C for uninjected oocytes and oocytes expressing Shaker and Shaker ILT (Fig. 4*F* and Fig. S5 *C* and *F*). Although these data do not rule out the additional involvement of other regions, they suggest that the pore domain of TRPV1 contains the structural elements that are required for activation by noxious heat with a similar sensitivity as the full-length TRPV1 channel.

To test whether pore domain mutants established to perturb gating in TRPV1 would cause similar perturbations in C11, we studied the F640L mutant that stabilizes the open state, causing partial constitutive activation of TRPV1, enhanced sensitivity to capsaicin, and heat-sensitive currents at lower temperatures than those required to activate the WT channel (16). For both TRPV1 and the C11 chimera, we observed that the mutation caused partial constitutive activation of the channel at room temperature (Fig. 5 *A* and *B*), could be further activated by capsaicin or K2K2 (Fig. 5 *A* and *B*), and displayed clearly altered responses to heating (Fig. 5 *C* and *D*). From these results, we conclude that the F640L mutant similarly stabilizes the open state of the pore domain in both TRPV1 and the C11 chimera.

Discussion

Taken together, our results demonstrate that the pore domain of the TRPV1 channel is a bona fide protein domain because it can be transplanted into the Shaker Kv channel without disrupting many functional properties of TRPV1 that have been attributed to the pore domain. Our C11 chimera retains activation by K2K2 and DkTx, has a higher permeability for small monovalent cations relative to $NMDG^+$, and is permeable to Ca^{2+}. This chimera is not robustly activated by external protons, even though protons are thought to bind within the outer pore (25, 47, 48). However, mutations outside the pore domain of TRPV1 can disrupt activation by protons (47), suggesting that transplantation of the pore from TRPV1 to Shaker might similarly perturb the allosteric network through which protons influence the closed-to-open equilibrium. Remarkably, the C11 chimera retains exquisite sensitivity to noxious heat, demonstrating that the pore domain of TRPV1 contains the elements required for producing steeply temperature-dependent activation. The steep increase in macroscopic current upon heating in TRPV1 arises from a steep increase in open probability rather than in the single channel conductance (8). Although we cannot distinguish between these two possibilities in our experiments with C11, we consider that the similarity in the temperature-activation relations between C11, TRPV1, and C23 makes it unlikely that their responses to heating arise from completely different mechanisms. Mutations throughout the sequence of TRPV and TRPA1 channels have been reported to alter activation of these channels by heat, including the pore domain (16, 17, 20, 49), the N-terminal Ankyrin-repeat domains (9, 10, 50–53), and the C terminus (12). However,

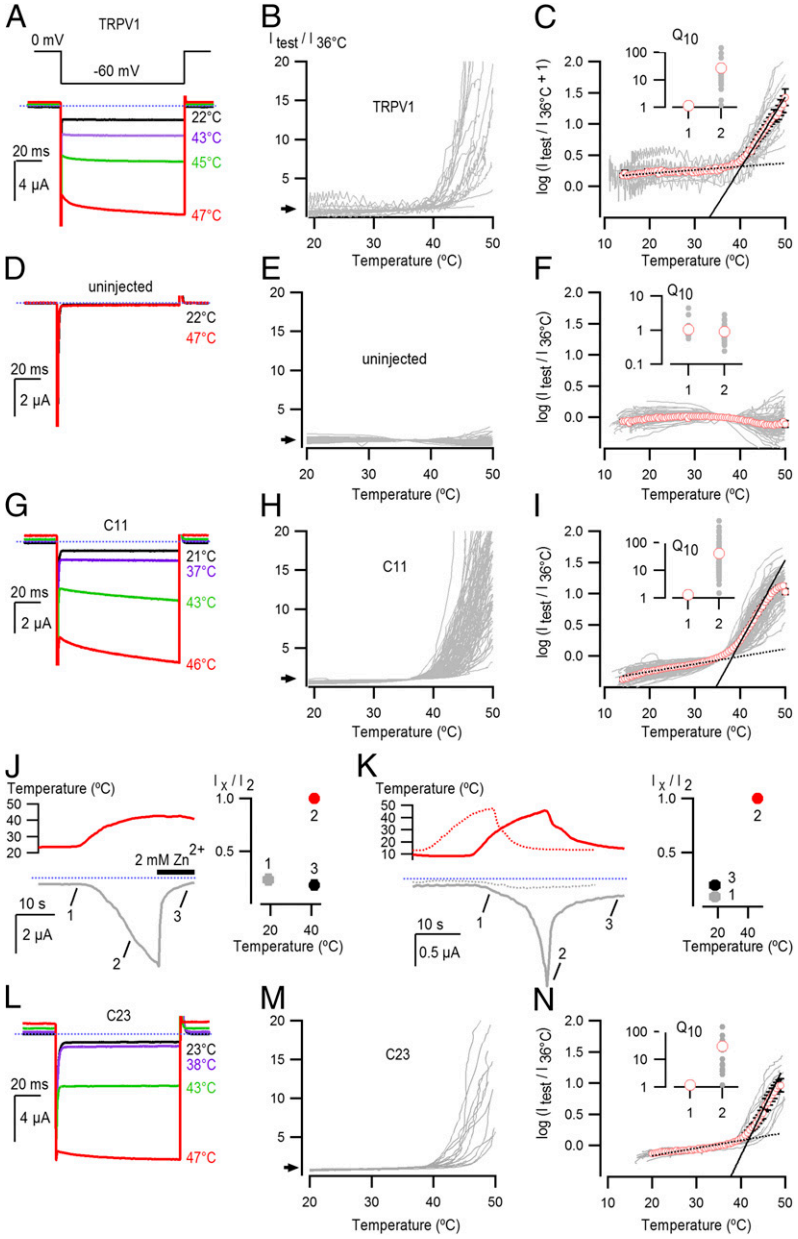

Fig. 4. Heat activation of TRPV1 and the C11 chimera. (*A*) Representative current traces for TPRV1-expressing cells activated by heating. Pulses from 0 to −60 mV were given at 2 Hz. (*B*) Current vs. temperature relations at −60 mV obtained from experiments as in *A* for temperatures from 20 °C to 50 °C, with the mean current values at the end of each pulse to −60 mV displayed as a line graph. Individual cells are shown with currents normalized by their amplitude at 36 °C ($n = 24$). (*C*) Plot of log ($I_{test}/I_{36\ °C} + 1$) obtained from the relations in *A* with the mean relation shown as red circles ± the SEM. The ratio of $I_{test}/I_{36\ °C}$ was offset by arbitrarily adding a value of 1 to the data to avoid large distortions in the log curves at lower temperatures, resulting from having small leak currents where some data points are ≤0. The linear fit at low temperatures (dotted black line) had a Q_{10} of 1.1, while that at high temperatures (continuous black line) had a Q_{10} of 26.8. The *Inset* shows Q_{10} values for low and high temperatures from fits to data from individual cells (gray circles) and red circles representing the mean values ± the SEM in black. (*D–F*) Representative current traces, temperature-activation relations, and Q_{10} determinations for cells not expressing exogenous channels ($n = 88$). (*G–I*) Representative current traces, temperature-activation relations, and Q_{10} determinations for cells expressing the C11 chimera ($n = 108$). The fit at low temperatures had a Q_{10} of 1.3, while that at high temperatures had a Q_{10} of 40.8. (*J*) Representative current time course for C11 obtained similarly as in *G*, showing Zn^{2+} block of temperature-activated currents. Temperature is shown in red on the *Upper Inset*, and it was increased from room temperature to ~42 °C, after which a solution supplemented with 2 mM Zn^{2+} at an equally high temperature was applied (denoted by the thick black horizontal line). The dotted blue line denotes the zero-current level. Data from a population of cells was pooled after normalizing the initial current at room temperature (*1*) and the current after Zn^{2+} application at high temperature (*3*) to the current at an equivalent temperature before Zn^{2+} application (*2*). The resulting mean ± SEM for both temperature and current (n = 4) are shown on the Inset to the right, where the y axis denotes normalized current and the *x* axis the temperature in which the pooled data were obtained. (*K*) Representative current time courses showing C11 (continuous gray curve) activation by heating, followed by deactivation upon cooling, obtained similarly to *G*. Temperature for the C11 experiment is shown as a continuous red curve at the *Top*. The dotted gray and red curves represent the current and temperature time courses for an uninjected oocyte from the same batch of oocytes as the C11 recordings. The blue dotted line denotes the zero-current level. Population data for C11 was pooled by normalizing the current at low temperature following heat activation (*3*) and the current at an equivalent temperature before heating (*1*) to the peak current measured at the maximal temperature (*2*), and is presented in the *Inset* on the *Right*. Data are shown as mean ± SEM for both temperature (*x* axis) and current (*y* axis) ($n = 3$). (*L–N*) Representative current traces, temperature-activation relations, and Q_{10} determinations for cells expressing the C23 chimera ($n = 16$). The fit at low temperatures had a Q_{10} of 1.2, while that at high temperatures had a Q_{10} of 29.8.

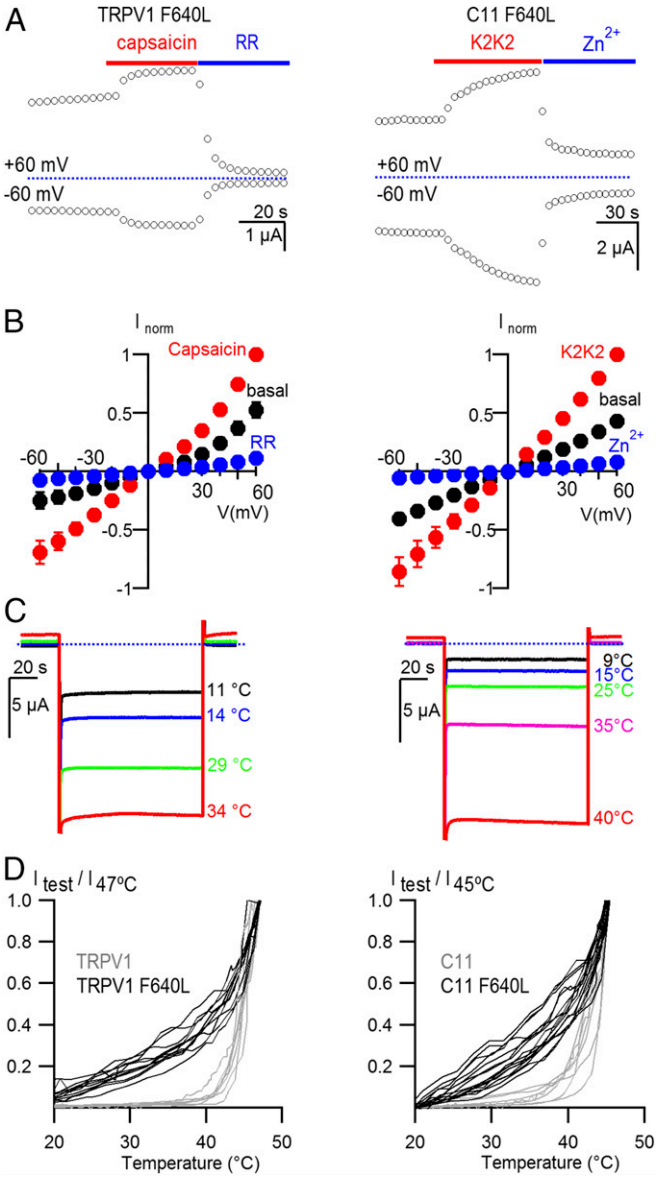

Fig. 5. A mutation within the pore domain of TRPV1 similarly alters gating of TRPV1 and the C11 chimera. (*A*) Time course for activation of membrane currents following application of capsaicin for cells expressing TRPV1 F640L (*Left*) or K2K2 for cells expressing C11 F640L (*Right*). Cells were held at −60 mV, and voltage was stepped to +60 mV for 100 ms every 3 s. TRPV1 was subsequently inhibited by RR (50 μM; *Left*) and the C11 chimera was inhibited by Zn^{2+} (2 mM; *Right*). (*B*) Normalized I–V relations for control (black symbols), capsaicin (10 μM, red symbols, *Left*), K2K2 (red symbols, *Right*), Ruthenium Red (10 μM, blue symbols, *Left*) or Zn^{2+} (2 mM; blue symbols, *Right*) obtained from experiments as in *A*. Currents were normalized to the amplitude of current in the presence of 10 μM capsaicin or 5 μM K2K2 at +60 mV (mean ± SEM for n = 3–5). (*C*) Representative current traces obtained by stepping from 0 mV to −60 mV for heat activation of TPRV1 F640L (*Left*) and C11 F640L (*Right*). (*D*) Temperature-activation relations for cells expressing TRPV1 (gray; n = 7), TRPV1 F640L (black; n = 11), C11 (gray; n = 7), and C11 F640L (black; n = 13). Constitutive current measured at low temperature (15 °C for TRPV1 and 20 °C for C11) was subtracted and currents were then normalized to the amplitude of current at 47 °C (TRPV1) or 45 °C (C11).

all of these perturbations in temperature-dependent activation could be explained by distant alterations in the allosteric network of interactions that regulate the gating mechanism of TRPV1. Even though our data cannot rule out the direct involvement of regions of the protein outside the pore in the process of temperature sensing, the pore domain in C11 seems to have comparable temperature sensitivity to TRPV1, indicating that it is a major contributor to the temperature-sensing mechanism. Consistently, two of the most robust perturbations in temperature activation have been established to target the pore domain of TRPV1, including the binding of external Na^+ ions and DkTx (19). The thermodynamic property driving activation of the heat sensor has been proposed to be the change in heat capacity arising from an increase in solvation of buried hydrophobic residues (23, 27). Interestingly, the cryo-EM structures of TRPV1 in closed and open states have revealed a cluster of hydrophobic residues behind the pore helix in TRPV1, nearby to where DkTx binds, that appears to become more solvent exposed when TRPV1 activates (5). This cluster is within the region of the pore transferred from TRPV1 into Shaker in the C11 chimera and contains residue F640, raising the possibility that it may function as the temperature sensor.

Materials and Methods

Structural Comparison of the Pore Domains of Kv and TRPV1 Channels. The crystal structure of the Kv1.2/2.1 paddle chimera [Protein Data Bank (PDB) ID code 2r9r] and the cryo-EM structure of the TRPV1 channel bound to RTx and DkTx (PDB ID code 5irx) were used to compare the structures of the pore domains of Kv and TRPV1 channels. Atomic coordinates for the pore domain (including S5, pore helix, and S6) of the Kv channel (R322–N410) and the TRPV1 channel (R575–N687) were superimposed and C_α rmsd and TM score calculated using TM align (28). TM scores range from 0 to 1 and unlike rmsd are not dependent on the size of the region being compared, with values above 0.5 indicating a high degree of structural similarity.

Expression Constructs and Molecular Biology. The rat TRPV1 channel (30) and the Shaker Kv channel (54) were kindly provided by David Julius, University of California, San Francisco, and Mark Tanouye, University of California, Berkeley, CA, respectively, and subcloned into the pGEM-HE vector (55). The Shaker-IR construct used here has a deletion of residues 6–46 to remove rapid inactivation (56, 57). 1D4 affinity tags (TETSQVAPA) were also added to the C termini of Shaker and C11 for biochemical detection of both proteins. Chimeras were generated by a three-step PCR protocol and mutations were introduced using a two-step PCR mutagenesis technique. The DNA sequence of all constructs and mutants was confirmed by automated DNA sequencing and cRNA was synthesized using T7/SP6 polymerase (mMessage mMachine kit, Ambion) after linearizing the DNA with appropriate restriction enzymes.

Biochemical Detection of Surface Expression. Four days after injection of cRNA, oocytes were incubated for 20 min at room temperature with sulfo-NHS-LC-biotin (0.5 mg/mL; ThermoFisher) in ND96 buffer containing (in millimoles): 96 NaCl, 2 KCl, 1.8 $CaCl_2$, 1 $MgCl_2$, 5 Na-Hepes, pH 7.6). After washing six times in ND96 buffer, 20 oocytes were homogenized in 400 μL of buffer H containing (in millimoles): 100 NaCl, 20 Tris·Cl, pH 7.4, 1% Triton X-100, 5 μL/mL protease inhibitor mixture (Sigma). Homogenization and all subsequent steps were performed at 4 °C. After centrifugation at 16,000 × g for 3 min, a 20-μL aliquot of the supernatant (total protein) was mixed with equal volume of 2× Laemmli sample buffer plus reducing agent: 50% 4× sample buffer (Bio-Rad), 10% 2-mercaptoethanol, 100 mM DTT. The remaining supernatant was diluted 1:1 with buffer H plus 50 μL of streptavidin agarose beads (ThermoFisher), then tumbled gently overnight at 4 °C. The streptavidin agarose beads were washed six times with buffer H with a 2-min centrifugation (16,000 × g) between each wash. At the end of the final wash, 40 μL of 1× Laemmli sample buffer plus reducing agent was added to the beads, and samples were heated at 70 °C for 10 min. Following a 2-min centrifugation (16,000 × g), the supernatant (surface protein) and total protein (collected earlier) were separated in 4–15% Mini-Protean TGX gel (Bio-Rad) using a running buffer containing (in millimoles): 25 Tris pH 8.3, 192 glycine, 0.1% SDS. Dual Color Precision Plus (Bio-Rad) was used as the protein molecular weight marker. Protein in the gel was transferred to nitrocellulose membrane (Bio-Rad) using 1× Trans-Blot Turbo 1× transfer buffer (Bio-Rad). The nitrocellulose membrane was probed with mouse anti-Rho 1D4 antibody (University of British Columbia) diluted 1:2,000 in TBS-T containing (in millimoles): 25 Tris, 137 NaCl, 3 KCl, 0.05% Tween-20, and expression was detected using Immobilon ECL Western detection reagents (Millipore).

Functional Characterization of Chimeras Between Shaker and TRPV1. In most experiments, His-tagged K2K2 was used to activate chimeras containing the pore domain of TRPV1 because the two K2 knot enhance the apparent affinity of the toxin and the His tag enhances its aqueous solubility and facilitates purification.

For experiments in Fig. S3, the C11 chimera was activated using His-tagged DkTx. His-tagged K2K2 and DkTx were produced as recombinant proteins and purified using HPLC as previously described (5). AgTx-2 was synthesized by peptide synthesis, folded in vitro, and purified by HPLC as previously described (58). All channel constructs were expressed in *Xenopus* oocytes and studied following a 1- to 4-d incubation after cRNA injection (incubated at 17 °C in 96 mM NaCl, 2 mM KCl, 5 mM Hepes, 1 mM $MgCl_2$ and 1.8 mM $CaCl_2$, 50 μg/mL gentamycin, pH 7.6 with NaOH) using the two-electrode voltage-clamp recording technique (OC-725C, Warner Instruments) with a 150-μL recording chamber. Data were filtered at 1 kHz and digitized at 5–10 kHz using pClamp software (Molecular Devices). Microelectrode resistances were 0.1–1 MΩ when filled with 3 M KCl. For recording macroscopic membrane currents in most experiments, the external recording solution contained (in millimoles/liter): 100 KCl, 10 Hepes, pH 7.6 with KOH at room temperature (~22 °C). For experiments to assess the Ca^{2+} permeability of the C11 chimera and TRPV1, Ca^{2+} (1 or 3 mM) was added to the external solution. In some experiments, 50 nL of 40 mM BAPTA was injected to prevent activation of calcium-activated chloride currents. If we assume an oocyte volume of 500 nL, the final intracellular concentration of BAPTA would be ~4 mM.

For temperature-activation experiments, calcium-activated chloride currents were minimized by using calcium-free solution containing 30 μM Caccinh-A01. External solutions were passed through glass capillary spirals immersed in a water bath maintained at about 70 °C, and recordings were performed during constant perfusion with temperature measured using a thermistor located close to the cell. Oocytes expressing TRPV1 and C11 were only studied if uninjected oocytes from the same batch contained a low density of endogenous temperature-sensitive currents at negative membrane voltages. For experiments testing for Zn^{2+} inhibition (Fig. 4*J*) or reversibility of temperature-activated currents (Fig. 4*K*) we used several perfusion lines to rapidly perfuse Zn^{2+} ions at high temperature or cold solution in which the perfusion capillaries were passed through a bath of ice water before reaching the recording chamber. Q_{10} values were obtained from $Q_{10} = 10^{10\times m}$, where m is the linear slope of $\log(I/I_{37\,°C})$ vs. T relations calculated either between ~15 and 35 °C or 38 and 50 °C. In the case of TRPV1 and C11 data, the ranges for the linear fits were chosen manually for each experiment so that they would capture the longest temperature interval >38 °C that had the largest steepness. For the control relations (i.e., uninjected oocytes and oocytes injected with Shaker and Shaker ILT) the two temperature intervals were fixed and the fits were done automatically using a script for IgorPro 6.34A (Wavemetrics). There were no differences in using the automated vs. manual fitting for the control data, which was essentially temperature independent. The mean log(I) vs. T curves were calculated by automatically binning each of the recordings in temperature intervals of 0.5 °C, and averaging a single data point within each interval per cell.

ACKNOWLEDGMENTS. We thank Alex Chesler, Joe Mindell, Shai Silberberg, Gilman Toombes, and members of the K.J.S. laboratory for helpful discussions; and Edoardo Sarti for assistance with TM-align. This work was supported by the Intramural Research Programs of the National Institute of Neurological Disorders and Stroke (NINDS), NIH (to K.J.S.), by a NINDS Competitive Postdoctoral Fellowship and K99 Career Development Award (to A.J.-O.), and by a grant from the Korea Research Institute of Bioscience and Biotechnology Research Initiative Program (Korean Biomedical Scientist Fellowship Program) (to C.B.).

1. Feng Q (2014) Temperature sensing by thermal TRP channels: Thermodynamic basis and molecular insights. *Curr Top Membr* 74:19–50.
2. Julius D (2013) TRP channels and pain. *Annu Rev Cell Dev Biol* 29:355–384.
3. Zheng J (2013) Molecular mechanism of TRP channels. *Compr Physiol* 3:221–242.
4. Gao Y, Cao E, Julius D, Cheng Y (2016) TRPV1 structures in nanodiscs reveal mechanisms of ligand and lipid action. *Nature* 534:347–351.
5. Bae C, et al. (2016) Structural insights into the mechanism of activation of the TRPV1 channel by a membrane-bound tarantula toxin. *Elife* 5:e11273.
6. Cao E, Liao M, Cheng Y, Julius D (2013) TRPV1 structures in distinct conformations reveal activation mechanisms. *Nature* 504:113–118.
7. Cao E, Cordero-Morales JF, Liu B, Qin F, Julius D (2013) TRPV1 channels are intrinsically heat sensitive and negatively regulated by phosphoinositide lipids. *Neuron* 77:667–679.
8. Liu B, Hui K, Qin F (2003) Thermodynamics of heat activation of single capsaicin ion channels VR1. *Biophys J* 85:2988–3006.
9. Cordero-Morales JF, Gracheva EO, Julius D (2011) Cytoplasmic ankyrin repeats of transient receptor potential A1 (TRPA1) dictate sensitivity to thermal and chemical stimuli. *Proc Natl Acad Sci USA* 108:E1184–E1191.
10. Yao J, Liu B, Qin F (2011) Modular thermal sensors in temperature-gated transient receptor potential (TRP) channels. *Proc Natl Acad Sci USA* 108:11109–11114.
11. Liu B, Qin F (2017) Single-residue molecular switch for high-temperature dependence of vanilloid receptor TRPV3. *Proc Natl Acad Sci USA* 114:1589–1594.
12. Brauchi S, Orta G, Salazar M, Rosenmann E, Latorre R (2006) A hot-sensing cold receptor: C-terminal domain determines thermosensation in transient receptor potential channels. *J Neurosci* 26:4835–4840.
13. Vlachová V, et al. (2003) Functional role of C-terminal cytoplasmic tail of rat vanilloid receptor 1. *J Neurosci* 23:1340–1350.
14. Joseph J, Wang S, Lee J, Ro JY, Chung MK (2013) Carboxyl-terminal domain of transient receptor potential vanilloid 1 contains distinct segments differentially involved in capsaicin- and heat-induced desensitization. *J Biol Chem* 288:35690–35702.
15. Saito S, et al. (2016) Evolution of heat sensors drove shifts in thermosensation between Xenopus species adapted to different thermal Niches. *J Biol Chem* 291: 11446–11459.
16. Myers BR, Bohlen CJ, Julius D (2008) A yeast genetic screen reveals a critical role for the pore helix domain in TRP channel gating. *Neuron* 58:362–373.
17. Grandl J, et al. (2010) Temperature-induced opening of TRPV1 ion channel is stabilized by the pore domain. *Nat Neurosci* 13:708–714.
18. Cui Y, et al. (2012) Selective disruption of high sensitivity heat activation but not capsaicin activation of TRPV1 channels by pore turret mutations. *J Gen Physiol* 139: 273–283.
19. Jara-Oseguera A, Bae C, Swartz KJ (2016) An external sodium ion binding site controls allosteric gating in TRPV1 channels. *Elife* 5:e13356.
20. Grandl J, et al. (2008) Pore region of TRPV3 ion channel is specifically required for heat activation. *Nat Neurosci* 11:1007–1013.
21. Wang H, Schupp M, Zurborg S, Heppenstall PA (2013) Residues in the pore region of Drosophila transient receptor potential A1 dictate sensitivity to thermal stimuli. *J Physiol* 591:185–201.
22. Kurganov E, Saito S, Tanaka Saito C, Tominaga M (2017) Requirement of extracellular Ca2+ binding to specific amino acids for heat-evoked activation of TRPA1. *J Physiol* 595:2451–2463.
23. Clapham DE, Miller C (2011) A thermodynamic framework for understanding temperature sensing by transient receptor potential (TRP) channels. *Proc Natl Acad Sci USA* 108:19492–19497.
24. Rosenbaum T, Gordon-Shaag A, Munari M, Gordon SE (2004) Ca2+/calmodulin modulates TRPV1 activation by capsaicin. *J Gen Physiol* 123:53–62.
25. Jordt SE, Tominaga M, Julius D (2000) Acid potentiation of the capsaicin receptor determined by a key extracellular site. *Proc Natl Acad Sci USA* 97:8134–8139.
26. Long SB, Tao X, Campbell EB, MacKinnon R (2007) Atomic structure of a voltage-dependent K+ channel in a lipid membrane-like environment. *Nature* 450:376–382.
27. Chowdhury S, Jarecki BW, Chanda B (2014) A molecular framework for temperature-dependent gating of ion channels. *Cell* 158:1148–1158.
28. Zhang Y, Skolnick J (2005) TM-align: A protein structure alignment algorithm based on the TM-score. *Nucleic Acids Res* 33:2302–2309.
29. Zhang F, et al. (2016) Engineering vanilloid-sensitivity into the rat TRPV2 channel. *Elife* 5:e16409.
30. Caterina MJ, et al. (1997) The capsaicin receptor: A heat-activated ion channel in the pain pathway. *Nature* 389:816–824.
31. Gross A, MacKinnon R (1996) Agitoxin footprinting the shaker potassium channel pore. *Neuron* 16:399–406.
32. Garcia ML, Garcia-Calvo M, Hidalgo P, Lee A, MacKinnon R (1994) Purification and characterization of three inhibitors of voltage-dependent K+ channels from Leiurus quinquestriatus var. hebraeus venom. *Biochemistry* 33:6834–6839.
33. Chung MK, Güler AD, Caterina MJ (2008) TRPV1 shows dynamic ionic selectivity during agonist stimulation. *Nat Neurosci* 11:555–564.
34. Miledi R (1982) A calcium-dependent transient outward current in Xenopus laevis oocytes. *Proc R Soc Lond B Biol Sci* 215:491–497.
35. De La Fuente R, Namkung W, Mills A, Verkman AS (2008) Small-molecule screen identifies inhibitors of a human intestinal calcium-activated chloride channel. *Mol Pharmacol* 73:758–768.
36. Lu Z, Klem AM, Ramu Y (2002) Coupling between voltage sensors and activation gate in voltage-gated K^+ channels. *J Gen Physiol* 120:663–676.
37. Lu Z, Klem AM, Ramu Y (2001) Ion conduction pore is conserved among potassium channels. *Nature* 413:809–813.
38. Jiang Y, Ruta V, Chen J, Lee A, MacKinnon R (2003) The principle of gating charge movement in a voltage-dependent K+ channel. *Nature* 423:42–48.
39. Jiang Y, et al. (2003) X-ray structure of a voltage-dependent K+ channel. *Nature* 423: 33–41.
40. Bosmans F, Martin-Eauclaire MF, Swartz KJ (2008) Deconstructing voltage sensor function and pharmacology in sodium channels. *Nature* 456:202–208.
41. Alabi AA, Bahamonde MI, Jung HJ, Kim JI, Swartz KJ (2007) Portability of paddle motif function and pharmacology in voltage sensors. *Nature* 450:370–375.
42. Gagnon DG, Bezanilla F (2009) A single charged voltage sensor is capable of gating the Shaker K+ channel. *J Gen Physiol* 133:467–483.
43. Bao H, Hakeem A, Henteleff M, Starkus JG, Rayner MD (1999) Voltage-insensitive gating after charge-neutralizing mutations in the S4 segment of Shaker channels. *J Gen Physiol* 113:139–151.
44. Voets T, et al. (2004) The principle of temperature-dependent gating in cold- and heat-sensitive TRP channels. *Nature* 430:748–754.
45. Yang F, Zheng J (2014) High temperature sensitivity is intrinsic to voltage-gated potassium channels. *Elife* 3:e03255.
46. Yao J, Liu B, Qin F (2010) Kinetic and energetic analysis of thermally activated TRPV1 channels. *Biophys J* 99:1743–1753.
47. Ryu S, Liu B, Yao J, Fu Q, Qin F (2007) Uncoupling proton activation of vanilloid receptor TRPV1. *J Neurosci* 27:12797–12807.
48. Ryu S, Liu B, Qin F (2003) Low pH potentiates both capsaicin binding and channel gating of VR1 receptors. *J Gen Physiol* 122:45–61.

49. Yang F, Cui Y, Wang K, Zheng J (2010) Thermosensitive TRP channel pore turret is part of the temperature activation pathway. *Proc Natl Acad Sci USA* 107:7083–7088.
50. Kang K, et al. (2011) Modulation of TRPA1 thermal sensitivity enables sensory discrimination in Drosophila. *Nature* 481:76–80.
51. Zhong L, et al. (2012) Thermosensory and nonthermosensory isoforms of Drosophila melanogaster TRPA1 reveal heat-sensor domains of a thermoTRP channel. *Cell Rep* 1: 43–55.
52. Gracheva EO, et al. (2011) Ganglion-specific splicing of TRPV1 underlies infrared sensation in vampire bats. *Nature* 476:88–91.
53. Gracheva EO, et al. (2010) Molecular basis of infrared detection by snakes. *Nature* 464:1006–1011.
54. Kamb A, Tseng-Crank J, Tanouye MA (1988) Multiple products of the Drosophila Shaker gene may contribute to potassium channel diversity. *Neuron* 1:421–430.
55. Liman ER, Tytgat J, Hess P (1992) Subunit stoichiometry of a mammalian K+ channel determined by construction of multimeric cDNAs. *Neuron* 9:861–871.
56. Zagotta WN, Hoshi T, Aldrich RW (1990) Restoration of inactivation in mutants of Shaker potassium channels by a peptide derived from ShB. *Science* 250:568–571.
57. Hoshi T, Zagotta WN, Aldrich RW (1990) Biophysical and molecular mechanisms of Shaker potassium channel inactivation. *Science* 250:533–538.
58. Milescu M, Lee HC, Bae CH, Kim JI, Swartz KJ (2013) Opening the shaker K+ channel with hanatoxin. *J Gen Physiol* 141:203–216.